Journal of Structural Biology 197 (2017) 155–162

Contents lists available at ScienceDirect

Journal of Structural Biology

journal homepage: www.elsevier.com/locate/yjsbi

Imaging complement by phase-plate cryo-electron tomography from initiation to pore formation

Thomas H. Sharp [a,*], Frank G.A. Faas [a], Abraham J. Koster [a,b], Piet Gros [c,*]

[a] Section Electron Microscopy, Department of Molecular Cell Biology, Leiden University Medical Center, 2300 RC Leiden, The Netherlands
[b] NeCEN, Gorlaeus Laboratories, Leiden University, 2333 CC Leiden, The Netherlands
[c] Crystal and Structural Chemistry, Bijvoet Center for Biomolecular Research, Department of Chemistry, Faculty of Science, Utrecht University, Padualaan 8, 3584 CH Utrecht, The Netherlands

ARTICLE INFO

Article history:
Received 24 May 2016
Received in revised form 17 August 2016
Accepted 13 September 2016
Available online 20 September 2016

Keywords:
C1
Complement
Electron tomography
Membrane attack complex
Phase plate

ABSTRACT

Phase plates in cryo-electron tomography (cryoET) improve contrast, increasing the ability to discern separate molecules and molecular complexes in dense biomolecular environments. Here, we applied this new technology to the activation of the human complement system. Binding of C1 to antigen-antibody complexes initiates a cascade of proteolytic events that deposits molecules onto adjacent surfaces and terminates with the formation of membrane-attack-complex (MAC) pores in the targeted membranes. We imaged steps in this process using a Volta phase plate mounted on a Titan Krios equipped with a Falcon-II direct electron detector. The data show patches of single-layer antibodies on the surface and C1 bound to antibody platforms, with ca. ~4% of instances where C1r and C1s proteases have dissociated from C1, and potentially instances of C1 transiently interacting with its substrate C4 or product C4b. Next, extensive deposition of C4b and C3b molecules is apparent, although individual molecules cannot always be properly distinguished with the current methods. Observations of MAC pores include formation of both single and composite pores, and instances of potential soluble-MAC dissociation upon failure of membrane insertion. Overall, application of the Volta phase plate cryoET markedly improved the contrast in the tomograms, which allowed for individual components to be more readily interpreted. However, variability in the phase shift induced by the phase-plate during the course of an experiment, together with incomplete sampling during tomogram acquisition, limited the interpretability of the resulting tomograms. Our studies exemplify the potential in studying molecular processes with complex spatial topologies by phase-plate cryoET.

1. Introduction

Cryo-electron tomography (cryoET) allows three-dimensional imaging of macromolecular structures up to several hundred nm in size yet with nm-scale resolution (Asano et al., 2016). In recent years, significant improvements of the instrumentation required for cryo-electron microscopy (cryoEM) have become available, in particular direct-electron detectors, highly stable cryo-electron microscopes, and the capacity for multi-day data collection (Cheng, 2015). Nevertheless, cryoEM inherently suffers from suppressed image contrast at low spatial frequencies that can only be partly restored by defocusing, which leads to reduced resolution (Erickson and Klug, 1971). Recently a phase plate (the Volta phase plate; VPP) became commercially available for cryoEM, which restores the low-frequency contrast (Danev et al., 2014), allowing in-focus data collection and single-particle analysis (Danev and Baumeister, 2016; Khoshouei et al., 2016), cryoET (Fukuda et al., 2015), and subtomogram averaging (Asano et al., 2015; Sharp et al., 2016). The resolution of cryo-tomograms, and subsequent sub-tomogram averages, is limited by frequency-dependent contrast reversals as described by the contrast transfer function (CTF) (Fernandez et al., 2006; Xiong et al., 2009). However, with a phase plate the need to generate low-frequency contrast by defocusing is no longer required, with the consequence that the frequency of the first contrast reversal is increased with respect to cryoET without a phase plate (Danev and Nagayama, 2001). This results in higher resolution tomograms with more contrast, facilitating their direct interpretation without subtomogram averaging

Abbreviations: CC, correlation coefficient; cryoEM/T, cryo-electron microscopy/tomography; CTF, contrast transfer function; DNP, 2,4-dinitrophenyl; FB, factor B; MAC, membrane attack complex; NHS, normal human sera/serum; VPP, Volta phase plate.

* Corresponding authors.
E-mail addresses: t.sharp@lumc.nl (T.H. Sharp), p.gros@uu.nl (P. Gros).

http://dx.doi.org/10.1016/j.jsb.2016.09.008
1047-8477/

(Fukuda et al., 2015). Recently, we applied phase-plate cryoET in combination with subtomogram averaging to visualize formation of the membrane-attack complex (MAC), the final stage of the complement pathway (Sharp et al., 2016). Herein, we use electron cryo-tomograms collected using a VPP to study the molecular distribution of complement components on synthetic cell mimics, and visualize the development of complement activation using depleted sera to block the linear cascade at discrete stages.

The mammalian complement system provides protection against invading microbes in blood or interstitial fluids by labeling them for destruction and induction of immune-cell responses, such as phagocytosis by macrophages and stimulation of B and T cells. The pathways of complement have been extensively reviewed, see e.g. (Bajic et al., 2015; Dunkelberger and Song, 2010; Merle et al., 2015a,b; Ricklin et al., 2010; Walport, 2001). In brief, the complement system consists of ca. 30 soluble plasma proteins and cell-surface receptors. In the presented study we focused on the plasma proteins of the complement system reacting with lipid bilayer surfaces, using synthetic liposomes as a model system (Yamamoto et al., 1995). Specifically, the classical pathway of complement activation is initiated on these liposomes by binding of antibodies to lipid-bound haptens, forming immune complexes on the liposome membrane. Next, the first complement component C1, a 790-kDa complex consisting of a hexameric recognition module C1q and a hetero-tetramer of proteases C1r and C1s, binds to the immune complexes, starting the proteolytic cascade of complement. The activated proteases C1s in C1 cleave both C4 and C2 forming a C4b2a complex (where "b" and "a" indicate cleavage products), which in turn cleaves C3 producing C3b. The homologous products C4b and C3b attach to the targeted microbes *via* reactive thioester moieties, which become exposed upon cleavage of C4 and C3, and covalently react with hydroxyl- and amino-groups on the microbial surface. This labeling, or opsonization, of the microbe is enhanced through a positive feedback loop in which protease factor B (FB) binds to C3b and is cleaved by factor D forming a C3bBb complex. This loop may also initiate complement via spontaneous hydrolysis of C3, known as the alternative pathway. Both C4b2a and C3bBb are C3 convertases, but additional deposition of C3b molecules can yield ternary complexes C4b3b2a and $C3b_2Bb$, which alter their substrate specificity from C3 to C5, hence forming C5 convertases. Cleavage of C5 marks the terminal pathway of complement activation. C5b associates with C6, C7, C8 and multiple copies of C9 forming the membrane-attack-complex (MAC), large ~100-Å wide pores, which lyse the microbial membrane.

Two previous papers (Diebolder et al., 2014; Sharp et al., 2016) demonstrated the potential of our model system for imaging complement initiation and MAC-pore formation. Here, we will report further results obtained in our efforts to provide a step-by-step visualization of complement activation on a membrane surface. These studies illustrate the major advances in cryoET using the recent technical developments, reveal its current limitations, and indicate the potential of imaging complex biological processes using cryoET.

2. Materials and methods

2.1. Complement activity assays

Purified protein, depleted sera and normal human sera (NHS) were purchased from Complement Technologies (Complement Technologies, Texas, USA) and stored at -80 °C. For complement activity assays, 2,4-dinitrophenyl (DNP)-labeled liposomes (Wako Diagnostics, Virginia, USA) were monitored at 340 nm using an Ultrospec 2100 pro (Biochrom Ltd., Cambridge, UK), as described (Yamamoto et al., 1995). Sera were used at final concentrations of 2.5 vol%. Depleted sera were reconstituted with the respective purified protein at the following concentrations prior to assay: C2, 0.02 mg/ml; C4, 0.4 mg/ml; C3, 1.2 mg/ml; C5, 0.075 mg/ml (Morley and Walport, 2000).

2.2. Cryo-electron tomography

Liposomes were mixed with antibodies and sera as described above and vitrified as described in (Sharp et al., 2016). A Tecnai T20 (FEI Company, Eindhoven, NL) equipped with a field emission gun operating at 200 kV was used to acquire tilt series without a phase plate, which were imaged at × 29 k magnification on a Gatan Ultrascan 4 k charged coupled device (Gatan, Inc., Abingdon, UK) binned 2×, for a final pixel size of 0.79 nm, using a tilt scheme from −60° to +60° in 2° increments. Focussing to −6000 nm was performed prior to each image acquisition using low-dose conditions. The total dose for each tomogram was ~6100 e^-/nm^2. Tilt-series collected with the phase plate were acquired using a Titan Krios transmission electron microscope (FEI Company, Eindhoven, NL) equipped with a field emission gun operating at 300 kV. Alignment of beam-shift pivot points and on-plane illumination was performed prior to imaging. A Volta phase plate (FEI, Eindhoven, The Netherlands), heated to 225 °C, was conditioned for 300 s with a dose of 0.17 nA for a final charge of ca. 50 nC to generate an approximate phase shift of 90°. The VPP was advanced to a new area before the acquisition of each tilt series, and allowed to settle for 300 s before re-conditioning. The phase plate was also conditioned for an additional 10 s between each tilt image. Discontinuous tilt series were collected using Tomography 4.0 (FEI Company, Eindhoven, The Netherlands) at ×29 k magnification using a tilt scheme from 0° to −60° before collecting 0° to +60°, in 2° increments. Total dose for the tilt series was 6100 e^-/nm^2. Focusing to −500 nm was performed prior to each image acquisition using a low-dose routine.

2.3. Tomogram processing

Tomograms were semi-automatically processed with batchruntomo from the software program IMOD (Mastronarde and Held, 2017) using fiducial-based tracking methods. For tilt series acquired without the phase plate, CTF determination was performed using the software program TomoCTF (Fernandez et al., 2006) and corrected using ctfphaseflip within IMOD (Xiong et al., 2009). For tilt series acquired with the phase plate, no CTF correction was performed. Gold fiducials were erased after alignment prior to reconstruction. Tomograms were reconstructed using eight iterations of the simultaneous iterative reconstruction technique (SIRT).

Electron microscopy density maps EMD-2507 (Diebolder et al., 2014) and EMD-3289 (Sharp et al., 2016) were used for C1 and the MAC pore, respectively. Maps were fit into tomogram volumes using the "fit-in-map" routine from UCSF Chimera (Pettersen et al., 2004). Isosurfaces representations were de-noised for clarity by hiding disconnected particles smaller than 2000 voxels using the command "hide dust" within UCSF Chimera. Particles were colored by correlation coefficient (CC), and colors were normalized to the highest CC in each tomogram from blue (highest) to red (CC = 0): since the missing wedge is present in tomograms but not in subtomogram averages the maximum CC did not achieve unity. The C1s domains were modeled using crystal structure 4J1Y (Perry et al., 2013) and manually oriented in the tomograms. All images and movies were made with UCSF Chimera (Pettersen et al., 2004).

3. Results and discussion

3.1. Phase plate imaging enhances tomographic interpretation

We first imaged complement activation on antigenic liposomes, both with and without the phase plate, 20 min after initiation (Fig. 1). No protein binding was observed by phase plate cryoET without antibody-mediated complement activation (Fig. 1A). In contrast, activation of complement by NHS yielded a dense layer of ca. 10–12 nm of deposited proteins on the liposomes (Fig. 1B). The large C1 complexes extending beyond the dense protein layer (white arrowheads, Fig. 1B), as well as large MAC pores perforating the membrane (black arrowheads, Fig. 1B) are apparent in tomograms obtained without phase plates. Results obtained from data collected using the VPP are shown in Fig. 1C. C1 complexes (white arrowheads; Fig. 1C) and MAC pores (black arrowheads; Fig. 1C) are more distinct and show more features than without the phase plate. For example, the initiating C5b6 complex of the MAC pore can be identified on top of the pore barrel (asterisk; Fig. 1C), and Fab arms of antibodies bound to the surface below the C1 complexes can be discerned. Whilst these antibody-C1 complexes have been described previously (Diebolder et al., 2014), the phase plate and direct-electron detector allow individual particles to be interpreted more readily without the previous requirement for dual-tilt reconstruction and sub-tomogram averaging.

The enhancement of contrast generated by the VPP (Fig. 2A) depends on the electron dose irradiating a small spot on the phase plate to generate the phase shift, known as conditioning (Danev et al., 2014). Whilst conditioning of the phase plate is directional and advances the phase shift, we observed both increasing (Fig. 2B) and decreasing contrast (Fig. 2C) over the course of tilt series acquisition. This increase in phase is primarily due to continuous dose-dependent phase-plate conditioning from multiple exposures during tracking, focussing and acquisition, leading to an increase in contrast (Danev et al., 2014). However, the decrease in contrast is less easily described. As reported by Danev, et al. after conditioning, the phase shift recovers over the course of days (Danev et al., 2014), however we observe decreasing phase shift over the course of acquisition (minutes to hours). This can be explained by mechanical instability ("drifting") of the VPP, which will result in misalignment of the conditioned area on the VPP and a decrease in contrast. Although mechanical instability would result in the effects described, we do not rule out other factors causing these phase shift fluctuations.

Whilst phase-plate cryoET increased the contrast and interpretability of tomographic reconstructions (Fig. 1), the resolution remained limited by the CTF. However, the phase plate also generates intermediate resolution tomograms without the requirement for CTF correction (Asano et al., 2015; Sharp et al., 2016) and as such we performed no CTF-correction on tilt series collected with

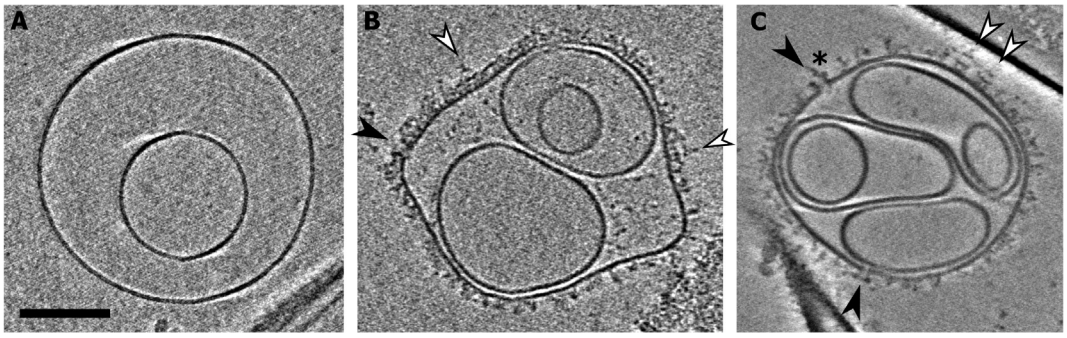

Fig. 1. Phase-plate imaging enhances the contrast of images showing complement components bound to liposome membranes in the presence of complement-activating antibodies. (A) A tomographic slice of an antigenic liposome in the presence of NHS but no antibodies. (B & C) Complement deposition imaged without (B) and with (C) the phase plate (different liposomes). White and black arrowheads indicate C1 molecules and MAC pores, respectively. All tomographic slices are 5 nm thick; samples were incubated for 20 min. Please note, data from (C) also appears in (Sharp et al., 2016). Scale bar is 100 nm.

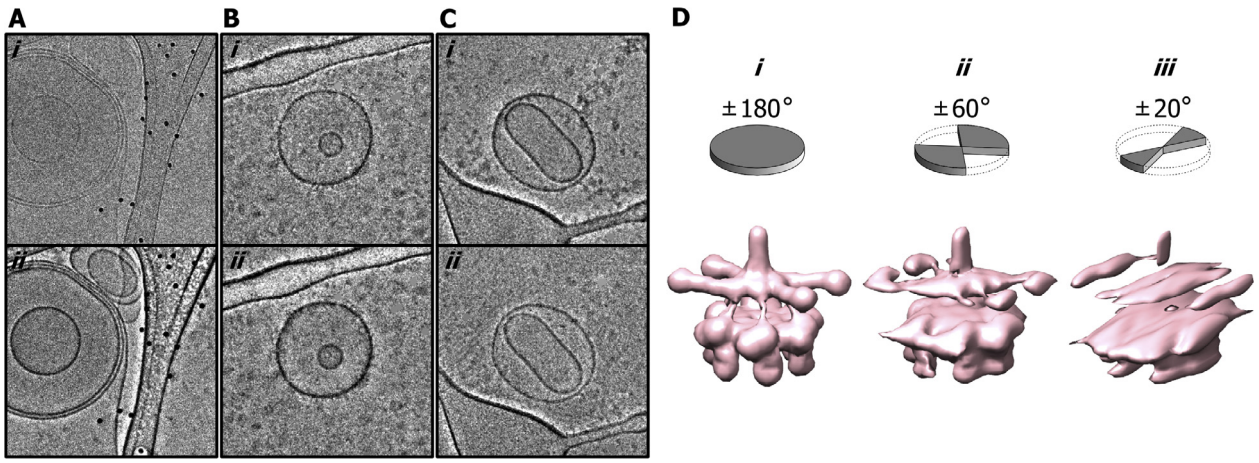

Fig. 2. Variations in contrast during tilt-series collection, and missing wedge effects, limits the resolution of phase plate tomograms. (A) Images of liposomes before (*i*) and after (*ii*) VPP conditioning displaying the increase in contrast. Also visible are lacey-carbon film and 10 nm gold fiducials. (B) Example tilt images showing the contrast continuing to increase between the start (*i*), and halfway through (*ii*) acquisition of a discontinuous tilt series. (C) Tilt images exhibiting a decrease in amplitude contrast between the start (*i*), and halfway through (*ii*) a discontinuous tilt series. (D) Antibody-C1 model modified from (Diebolder et al., 2014) demonstrating how the completeness of data collection (grey circles, top) directly affects the anisotropic resolution of the reconstruction and subsequent interpretability (pink maps, bottom).

the phase plate in this study. Although CTF-correction may increase the resolution of tomograms, accurate CTF determination of cryoET tilt series is non-trivial (Fernandez et al., 2006; Xiong et al., 2009), and further hindered by the dose-dependent phase shift from the VPP (Fig. 2). Each tilt image is therefore transmitted with a unique amplitude-contrast value and hence a unique CTF, which complicates CTF determination. Ideally, tilt series would be collected in-focus to maximise the possible resolution without CTF-correction; however, a defocus of −500 nm was applied so that images acquired with a phase shift ≠ 90° still contained sufficient low-frequency contrast for alignment.

The achievable resolution of subtomogram averages derived from tomograms collected using the VPP can be improved by employing a reconstruction using only low tilt-angles (Khoshouei et al., 2017). Incomplete sampling during tilt-series acquisition, however, creates a "missing wedge" of data, resulting in anisotropic resolution and reducing the interpretability of the tomogram (Fig. 2D). Full data collection (Fig. 2D *i*) would yield a 3D map with isotropic resolution. Data collection from ±60° (Fig. 2D *ii*) and ±20° (Fig. 2D *iii*) results in a map "smeared" perpendicular to the missing wedge and in proportion to the amount of missing data. We collected tilt-series from ±60° to minimize missing wedge artefacts, reducing anisotropy and increasing the interpretability of the tomographic volume. Although this interpretation remains limited by the aforementioned missing wedge of data, individual complement components can be more reliably identified and their orientation and spatial distribution revealed with greater accuracy.

3.2. A molecular atlas for the classical complement pathway

Next, using phase-plate cryoET, we imaged the cascade of molecular events that unfold on liposomal surfaces upon antibody-mediated complement activation. Addition of polyclonal goat anti-DNP antibodies and normal human sera (NHS) to DNP-carrying liposomes induced MAC formation and subsequent liposome lysis (Yamamoto et al., 1995) (Fig. 3A). Maximal lysis rates were observed after 10–20 min (Fig. 3B), we therefore chose to vitrify liposomes 20 min after complement activation. Complement component depletion effectively inhibited liposome lysis (Fig. 3A), whereas reconstitution of depleted sera with the respective purified protein restored complement activity (Fig. 3A). Thus, for example, using serum depleted of C4 is effectively equivalent to adding purified C1 (Diebolder et al., 2014). By using these depleted sera to block the linear pathway at specific stages, we mimicked the temporal resolution lacking in EM, which enables imaging of the progression of the complement cascade with molecular detail using phase plate cryoET.

We collected phase-plate tomograms of the separate steps in the proteolytic cascade to visualize how complement develops on a lipid bilayer. Fig. 4A shows tomographic slices at eight stages of complement activation. Using the same model system, two previous cryoET studies already reported C1 binding to antibodies, performed without a phase plate (Diebolder et al., 2014), and formation of MAC complexes, which benefitted greatly from the increased contrast afforded by the phase plate (Sharp et al., 2016). As described previously, no protein binding to liposomes is observed in NHS without addition of antibodies (Fig. 4A *i*) (Sharp et al., 2016). Thus, neither auto-activation through C3 hydrolysis (of the so-called alternative pathway of complement activation) occurs on these surfaces, in agreement with the absence of lysis in the absence of antibodies (Fig. 3), nor binding of soluble regulators factor H and C4BP occur within 20 min prior to cryo-fixation. Tomographic slices obtained with phase-plate cryoET showed more clearly density corresponding to antibody platforms ~10 nm above the liposome surface (Fig. 4A *ii*), cf. data obtained without using a phase plate by Diebolder et al. (2014). Moreover, the large C1 complexes on top of the antibody layer, studied by Diebolder et al. (2014), became more clearly visible (Fig. 4A *iii*). Increased liposome opsonization in the presence of C2- and C3-depleted sera was also visible, although distinguishing C4b molecules from bound antibodies was not always possible (Fig. 4A *iv* & *v, resp.*). Differentiating C4b and C3b was not possible (Fig. 4A *vi*), and would require very high resolution to do so, due to their structural homology. Furthermore, we could not discern increased C3b deposition through the amplification loop of the alternative pathway (Fig. 4A *vii*), although this may be possible following statistical analysis comparing an increased number of tomograms of both FB- and C5-depleted sera. Moreover, we cannot discern C3 or C5 convertases (C4b2a/C3bBb and C4b3b2a/C3b$_2$Bb resp.) on the liposomes, which might be due to the anisotropic resolution of the tomograms or possibly due to the inherent dissociation of the convertases. Finally, MAC complexes initiated upon C5 cleavage by the C5 convertases are readily discernable in tomographic slices of both FB-depleted and NHS (Figs. 4A *vi* & *viii*), as previously described (Sharp et al., 2016).

Fig. 4B displays "molecular atlases" of the tomograms shown in Fig. 4A (see also Movies S1-6). These views have been simplified by isosurface rendering and de-noising by hiding disconnected

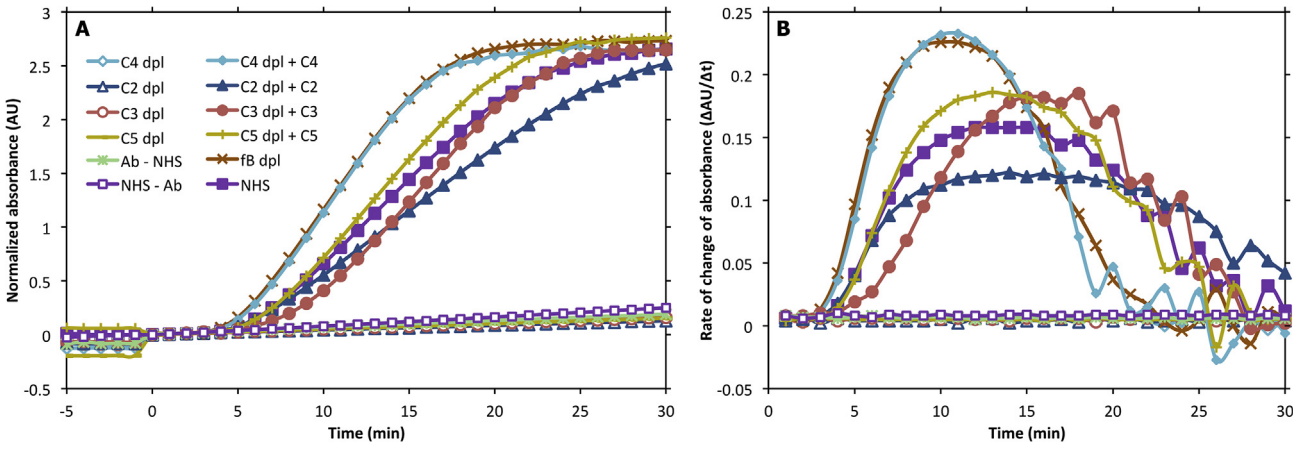

Fig. 3. Depleting human sera of specific complement components blocks MAC-mediated lysis of liposomes, which can be reconstituted with the respective purified protein. (A) Time-resolved absorbance of reduced nicotinamide adenine dinucleotide (NADH) produced after MAC-mediated lysis of liposomes. Lysis is blocked by omitting NHS, antibodies, or depleting sera of complement components C4, C2, C3, or C5. NHS, FB-depleted sera and reconstituted sera are able to lyse liposomes. (B) Rate of change of absorbance after activation (1st derivative of (A)).

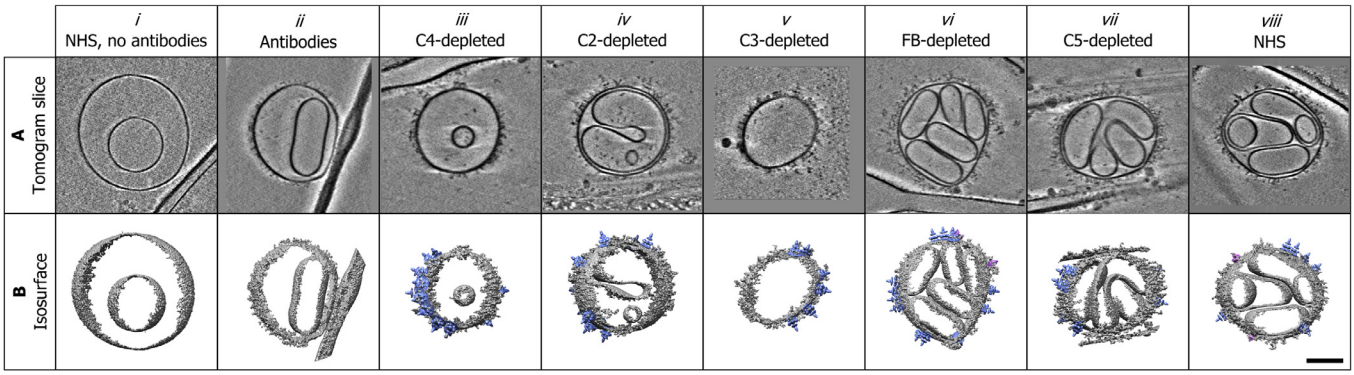

Fig. 4. Phase plate cryoET combined with sera depleted of specific complement components provides snapshots of complement activation on liposomes and the construction of molecular atlases. (A) Tomogram slices 5 nm thick and (B) isosurface renderings of tomograms shown in (A) for discrete steps of the classical complement pathway. Fitted 3D EM maps for C1 complexes are shown as blue, MAC pores as purple, liposome membranes and protein opsonization are colored grey. See also Movies S1–S6 corresponding to *iii-viii*, respectively. Scale bar is 100 nm.

densities not associated with the liposomes. Liposome-membrane and membrane-associated density have been colored grey, whilst light-blue and purple objects respectively indicate EM maps of C1-antibody complexes and MAC pores semi-automatically fitted into the tomograms. Fig. 4B *iii-viii* show the spatial distribution of these complexes as they occur on the individual liposomes. Overall, these data indicate the concept of developing molecular atlases, which are in addition to the focused studies on antibody-mediated initiation of the classical pathway (Diebolder et al., 2014) and MAC formation in the terminal pathway (Sharp et al., 2016). Below, we present further instances and aspects of studying complement activation using phase-plate cryoET, which show both the potential and current limitations of this approach.

3.3. Identifying surface-bound $C1qr_2s_2$ complexes and domains

Fig. 5A–C shows the binding of C1 complexes to antibodies on the liposome surfaces. The densities observed in Fig. 5A indicate individually bound antibodies up to contiguous patches of single layers of antibodies (of ~10-nm height), as reported by Diebolder et al. (2014). Interpretation of the molecular arrangement within these polyclonal antibody layers is, however, still limited by anisotropic resolution. Nevertheless, the layers are not ubiquitous, and antibodies also form more discrete structures on the liposomes. Addition of C4-depleted sera yields C1 binding to the surface-bound antibodies (Fig. 5A). Based on 11 tomograms of C4-depleted sera *versus* 5 tomograms of anti-DNP antibodies in the presence of liposomes (i.e. without NHS added), C1 binding decreases the extent of antibody oligomerization, as we observe C1 bound to isolated platforms (Fig. 5B). This may be indicative of C1q binding disrupting antibody arrays. Moreover, we observe both isolated and clustered antibody-C1 complexes (Fig. 5B & Movie S1). Whether this clustering reflects merely the breaking up of a previous extended antibody layer by multiple C1 complexes or is functionally relevant in C1 activation, such as the proposed intermolecular "cross" activation of MBL-MASP complexes by Degn et al. (2014), remains to be established.

Phase-plate imaging of C1 reveals structural details that are not visible by conventional cryoET. Individual collagen arms linking the hexameric C1q stalk domain to the C1q globular heads bound to the antibody platform are discernable in Fig. 5C. Moreover, both complete C1, i.e. $C1qr_2s_2$, complexes and C1q without $C1r_2s_2$ heterotetramer bound are visible (Fig. 5B, C & D). Only in a minority of cases (2 out of 45) we observed 'empty' C1q *versus* complete C1 bound on the antibodies (Fig. 5C) in the presence of C4-depleted sera.

The next step in the complement cascade, i.e. cleavage of C4 into C4b by the C1s proteases of the C1 complex, is achieved when using C2 depleted sera. Fig. 6 shows instances of C1 molecules with small globules on protruding arms, which possibly represent the serine protease domains (MW ~37 kDa) connected to the N-terminal $C1r_2s_2$ platforms bound to C1q (Bally et al., 2009; Phillips et al., 2009) (see also Movie S2). Alternatively these densities may correspond to a C1q globular head (MW ~46 kDa) on their collagen tails that are somehow not bound to the antibody platform, in agreement with the marked disorder observed by Diebolder et al. (2014). The protruding arms in Fig. 6C are observed to be bound to membrane-associated densities. These densities

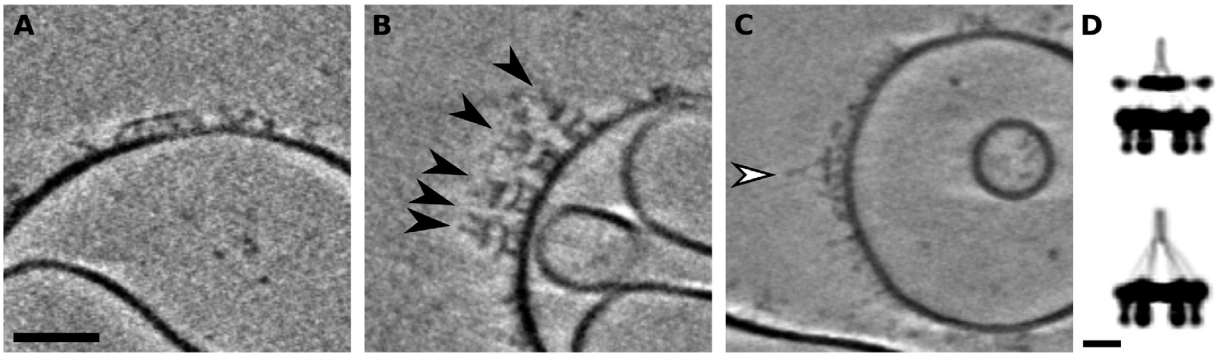

Fig. 5. Antibodies form extended layers and isolated platforms in the absence and presence of C1, respectively. (A) Tomogram slices of liposomes in the presence of antibodies showing extended antibody platforms when no complement components are present. (B) On addition of C4-depleted sera, tomogram slices show isolated islands with C1 complexes on top (black arrowheads). See also Movie S1. (C) C1q molecules without $C1r_2s_2$ present (white arrowheads) are also visible in tomogram slices. (D) Simulated projection of a model from (Diebolder et al., 2014) of $C1qr_2s_2$ (top) and C1q (bottom) bound to an antibody platform. All tomogram slices are 5 nm thick. Scale bars represent 50 nm (A, B & C) and 10 nm (D).

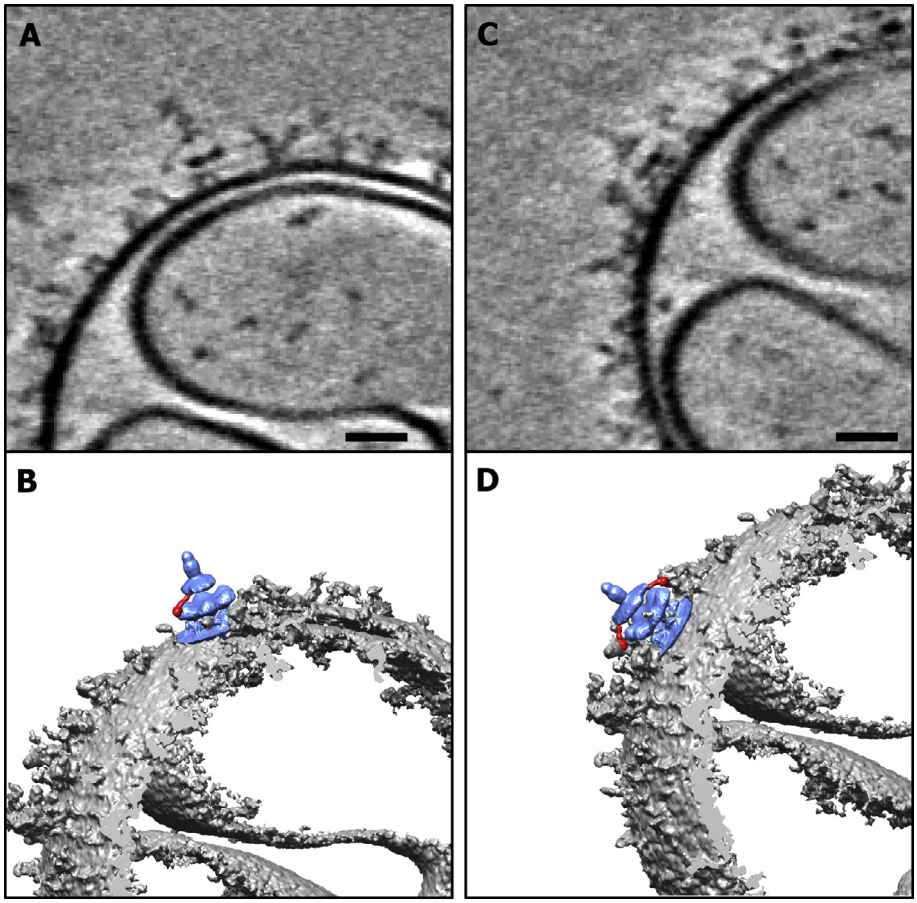

Fig. 6. Individual domains of C1 molecules can be interpreted in phase plate tomograms (see also Movie S2). (A & B) A 5 nm tomographic slice (A) showing density emanating from a C1 complex, interpreted in (B) as a single C1s domain (red) extending from the $C1r_2s_2$ platform of a C1 complex (blue). (C & D) A 5 nm tomographic slice (C) showing two opposing domains extending from a $C1r_2s_2$ platform bound to membrane-associated density, interpreted in (D) as two C1s domains (red). Scale bars represent 25 nm.

project further away from the liposome surface than the antibody platform, and as such it is possible that these represent opsonizing C4b molecules that have been cleaved, or C4 molecules that are in the process of being cleaved, by C1s serine proteases. These domains were not resolved by Diebolder et al. using subtomogram averaging (Diebolder et al., 2014), most likely because they are flexible. These phase-plate tomograms thus demonstrate the potential for *in situ* visualization of small, and/or flexible components of large protein complexes. For analysis of transient binding states, however, more individual observations of instances are required for a robust interpretation.

3.4. Single and multimeric MAC complexes

Phase-plate cryoET is a powerful technique to visualize *in situ* pore formation within native lipid bilayers, and determine both

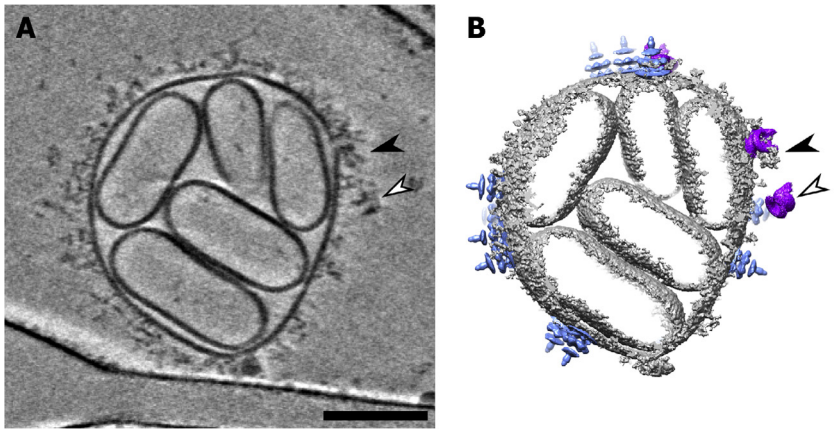

Fig. 7. A solution-phase MAC and MAC-associated density present after incubation with FB-depleted sera (see also Movie S4). (A) A 5-nm tomogram slice through a liposome incubated with antibodies and FB-depleted sera. Electron density associated with a MAC pore (black arrowhead), as well as a solution-phase MAC not inserted into the liposome membrane (white arrowhead), are visible. Please note, data from this tomogram also appears in (Sharp et al., 2016). (B) Isosurface representation of (A). Scale bar is 100 nm.

oligomeric states of pore complexes and 3D density maps of single pores (Sharp et al., 2016). Membrane-perforating MAC pores were visible in the presence of NHS and FB-depleted sera (Fig. 4 *vi* & *viii*, Movies S4 & S6), as well as purified C5b6, C7, C8 and C9 (Sharp et al., 2016). We have since observed MACs in solution under the same conditions (Fig. 7 and Movie S4), presumably following aborted membrane insertion and then dissociation. Heterogeneous initiating structures (C5b-7 and C5b-8) may act as nucleators for C9 polymerization, even if components are not stably inserted into membranes. Furthermore, two other composite MAC pores are observed on the same liposome (Fig. 7). At one position we observe a composite pore with additional density associated on the side (the identity of this density remains to be shown), and at a second position a composite dimeric pore with neighbouring C1 complexes is present. The latter arrangement perhaps suggests that multimeric pores (as previously reported (Sharp et al., 2016)), may arise locally, in addition to potential fusion from distantly created hemi-pores or prepores. However, given the resolution of these images mechanistic interpretations at this stage are highly speculative.

Thus, these data indicate that there is more to learn about pore formation and membrane perforation, and questions remain over the time course of events, for example; do MAC components form hemipores and prepores analogous to those formed by the cholesterol-dependent cytolysins (Leung et al., 2014)? Are composite pores formed from concatenation of diffusing hemipores? Phase-plate cryoET provides unprecedented data to help address these structural questions.

4. Conclusions

Utilizing the increased contrast afforded by the VPP has allowed us to image each step of the complement pathway at nm-scale resolution. The increased resolution and interpretability allows visualization of domains within protein complexes, such as individual C1 domains and C5b6 molecules. Furthermore, although single-particle analysis and subtomogram averaging can achieve sub-nanometer resolution, flexible domains and transient states are very hard to study and generally not well resolved when particles are averaged. Thus, phase-plate cryoET is therefore currently an optimal technique for gaining structural insights into transient stages of dynamical processes, such as occur in the complement pathway.

By employing antigenic liposomes as cell mimics, and using depleted sera to simulate the temporal component of complement, we have visualized extended antibody platforms that rearrange to form discrete islands during C1 binding; C1 complexes both with and without the $C1r_2s_2$ heterotetramer present; membrane opsonization by C4b and C3b; solution-phase MAC formation and formation of multimeric pores. Nevertheless, phase plate tomograms are still affected by the missing wedge and resulting anisotropic resolution, which limits interpretation and reduces the number of instances useful for interpretation and statistical analysis. In our opinion, the phase-plate cryoET method holds great potential for future research; in particular, when future developments would reduce the negative effects of the missing wedge and increase the stability of the phase-plate, as well as with more rigorous statistical analyses applied to the interpretation of the resulting tomograms.

These data taken together create a "molecular atlas" of complement. Although the study of any biochemical pathway is not complete without biochemical data and validation, this atlas provides a partial 3-dimensional overview for further research and can now be compared to modifications of complement protein activation, deposition and regulation, as well as lipid bilayer composition and environment.

Competing financial interests statement

The authors declare no competing financial interests.

Acknowledgements

This work was supported by the Council for Chemical Sciences (CW) of the Netherlands Organization for Scientific Research (NWO grant 700.57.010), the Netherlands Centre for Electron Nanoscopy (NeCEN), Leiden (NWO grant 175.010.2009.001) and by the Institute for Chemical Immunology, an NWO Gravitation project funded by the Ministry of Education, Culture and Science of the government of the Netherlands. F.G.A. Faas was supported by NanoNextNL of the Government of the Netherlands and 130 partners. We thank David Mastronarde for advice with IMOD and Suzan Rooijakkers for critical reading of the manuscript.

Appendix A. Supplementary data

Supplementary data associated with this article can be found, in the online version, at http://dx.doi.org/10.1016/j.jsb.2016.09.008.

References

Asano, S., Engel, B.D., Baumeister, W., 2016. In situ cryo-electron tomography: a post-reductionist approach to structural biology. J. Mol. Biol. 428, 332–343.
Asano, S., Fukuda, Y., Beck, F., Aufderheide, A., Forster, F., Danev, R., Baumeister, W., 2015. Proteasomes. A molecular census of 26S proteasomes in intact neurons. Science 347, 439–442.
Bajic, G., Degn, S.E., Thiel, S., Andersen, G.R., 2015. Complement activation, regulation, and molecular basis for complement-related diseases. EMBO J. 34, 2735–2757.
Bally, I., Rossi, V., Lunardi, T., Thielens, N.M., Gaboriaud, C., Arlaud, G.J., 2009. Identification of the C1q-binding sites of human C1r and C1s: a refined three-dimensional model of the C1 complex of complement. J. Biol. Chem. 284, 19340–19348.
Cheng, Y., 2015. Single-particle cryo-EM at crystallographic resolution. Cell 161, 450–457.
Danev, R., Nagayama, K., 2001. Transmission electron microscopy with Zernike phase plate. Ultramicroscopy 88, 243–252.
Danev, R., Baumeister, W., 2016. Cryo-EM single particle analysis with the Volta phase plate. Elife 5, e13046.
Danev, R., Buijsse, B., Khoshouei, M., Plitzko, J.M., Baumeister, W., 2014. Volta potential phase plate for in-focus phase contrast transmission electron microscopy. Proc. Natl. Acad. Sci. U.S.A. 111, 15635–15640.
Degn, S.E., Kjaer, T.R., Kidmose, R.T., Jensen, L., Hansen, A.G., Tekin, M., Jensenius, J.C., Andersen, G.R., Thiel, S., 2014. Complement activation by ligand-driven juxtaposition of discrete pattern recognition complexes. Proc. Natl. Acad. Sci. U.S.A. 111, 13445–13450.
Diebolder, C.A., Beurskens, F.J., de Jong, R.N., Koning, R.I., Strumane, K., Lindorfer, M. A., Voorhorst, M., Ugurlar, D., Rosati, S., Heck, A.J., van de Winkel, J.G., Wilson, I. A., Koster, A.J., Taylor, R.P., Saphire, E.O., Burton, D.R., Schuurman, J., Gros, P., Parren, P.W., 2014. Complement is activated by IgG hexamers assembled at the cell surface. Science 343, 1260–1263.
Dunkelberger, J.R., Song, W.C., 2010. Complement and its role in innate and adaptive immune responses. Cell Res. 20, 34–50.
Erickson, H., Klug, A., 1971. Measurement and compensation of defocusing and aberrations by Fourier processing of electron micrographs. Philos. Trans. R. Soc. Lond. B 261, 105–118.
Fernandez, J.J., Li, S., Crowther, R.A., 2006. CTF determination and correction in electron cryotomography. Ultramicroscopy 106, 587–596.
Fukuda, Y., Laugks, U., Lucic, V., Baumeister, W., Danev, R., 2015. Electron cryotomography of vitrified cells with a Volta phase plate. J. Struct. Biol. 190, 143–154.
Khoshouei, M., Pfeffer, S., Baumeister, W., Förster, F., Danev, R., 2017. Subtomogram analysis using the Volta phase plate. J. Struct. Biol. 197, 94–101.
Khoshouei, M., Radjainia, M., Phillips, A.J., Gerrard, J.A., Mitra, A.K., Plitzko, J.M., Baumeister, W., Danev, R., 2016. Volta phase plate cryo-EM of the small protein complex Prx3. Nat. Commun. 7, 10534.
Leung, C., Dudkina, N.V., Lukoyanova, N., Hodel, A.W., Farabella, I., Pandurangan, A. P., Jahan, N., Pires Damaso, M., Osmanovic, D., Reboul, C.F., Dunstone, M.A., Andrew, P.W., Lonnen, R., Topf, M., Saibil, H.R., Hoogenboom, B.W., 2014. Stepwise visualization of membrane pore formation by suilysin, a bacterial cholesterol-dependent cytolysin. Elife 3, e04247.
Mastronarde, D.N., Held, S.R., 2017. Automated tilt series alignment and tomographic reconstruction in IMOD. J. Struct. Biol. 197, 102–113.

Merle, N.S., Church, S.E., Fremeaux-Bacchi, V., Roumenina, L.T., 2015a. Complement system part I – molecular mechanisms of activation and regulation. Front. Immunol. 6, 262.
Merle, N.S., Noe, R., Halbwachs-Mecarelli, L., Fremeaux-Bacchi, V., Roumenina, L.T., 2015b. Complement system part II: role in immunity. Front. Immunol. 6, 257.
Morley, B.J., Walport, M.J., 2000. The Complement Facts Book. Academic Press, London.
Perry, A.J., Wijeyewickrema, L.C., Wilmann, P.G., Gunzburg, M.J., D'Andrea, L., Irving, J.A., Pang, S.S., Duncan, R.C., Wilce, J.A., Whisstock, J.C., Pike, R.N., 2013. A molecular switch governs the interaction between the human complement protease C1s and its substrate, complement C4. J. Biol. Chem. 288, 15821–15829.
Pettersen, E.F., Goddard, T.D., Huang, C.C., Couch, G.S., Greenblatt, D.M., Meng, E.C., Ferrin, T.E., 2004. UCSF Chimera–a visualization system for exploratory research and analysis. J. Comput. Chem. 25, 1605–1612.
Phillips, A.E., Toth, J., Dodds, A.W., Girija, U.V., Furze, C.M., Pala, E., Sim, R.B., Reid, K. B., Schwaeble, W.J., Schmid, R., Keeble, A.H., Wallis, R., 2009. Analogous interactions in initiating complexes of the classical and lectin pathways of complement. J. Immunol. 182, 7708–7717.
Ricklin, D., Hajishengallis, G., Yang, K., Lambris, J.D., 2010. Complement: a key system for immune surveillance and homeostasis. Nat. Immunol. 11, 785–797.
Sharp, T.H., Koster, A.J., Gros, P., 2016. Heterogeneous MAC initiator and pore structures in a lipid bilayer by phase-plate cryo-electron tomography. Cell Rep. 15, 1–8.
Walport, M.J., 2001. Complement. First of two parts. N. Engl. J. Med. 344, 1058–1066.
Xiong, Q., Morphew, M.K., Schwartz, C.L., Hoenger, A.H., Mastronarde, D.N., 2009. CTF determination and correction for low dose tomographic tilt series. J. Struct. Biol. 168, 378–387.
Yamamoto, S., Kubotsu, K., Kida, M., Kondo, K., Matsuura, S., Uchiyama, S., Yonekawa, O., Kanno, T., 1995. Automated homogeneous liposome-based assay system for total complement activity. Clin. Chem. 41, 586–590.